CALCULATION AND MEASUREMENT OF TRANSONIC FLOWS OVER AEROFOILS WITH NOVEL REAR SECTIONS

ICAS-88-3.10.2

P. R. Ashill
Royal Aircraft Establishment
Bedford MK41 6AE, UK

Abstract

A combined theoretical and experimental investigation into transonic flows over aerofoils of advanced design is described. The experiments have been performed at high subsonic speeds and over a wide range of Reynolds number up to 20 million on a number of aerofoils with rear pressure distributions of differing form and severity. Three families of aerofoils have been studied, all of which are of 14% thickness and have a high degree of rear camber. Data for aerofoil pressure distributions and overall forces are compared with predictions by a calculation method based on the viscous-inviscid interaction concept and including allowance in the modelling of the turbulent shear layers for effects which become important as separation is approached. Predictions of pressure distributions by this method are shown to be in generally good agreement with experiment for the various sections tested, and it is concluded that the method provides a reliable basis for designing aerofoil sections with advanced features.

1 Introduction

Computational Fluid Dynamics (CFD) methods for transonic flows over aerofoils have been shown to yield physically realistic solutions in a number of special cases generally with fully attached flow. However, these methods treat the shear layers approximately and hence further assessment is needed before the concepts involved can be extended with confidence to more complex flows. The need for such an assessment is particularly acute for flows at high subsonic speed over aerofoils of modern design having relatively large rear camber. For such flows, the adverse pressure gradients over the rear of the section can be particularly severe, leading to a rapid growth in boundary-layer thickness as the trailing edge is approached and possibly also to separation. Thus flows of this type, which are of great practical importance, pose a considerable challenge to the accuracy of the predictions by CFD methods.

This paper describes a combined theoretical and experimental investigation aimed at improving the modelling in a CFD method of flows approaching separation. The experiments were performed at high subsonic speeds in the 8ft × 8ft Pressurised Wind Tunnel at RAE Bedford on three families of aerofoils of 14% thickness and of modern design, some of which are novel in character.

Until fairly recently, the method most favoured in UK for calculating transonic flows over aerofoils was the viscous version of the Garabedian and Korn program (VGK)[1,2]. Based on the viscous-inviscid interaction concept, VGK uses a full-potential algorithm for the inviscid flow and integral methods to calculate the shear layers. VGK gives reasonable predictions of aerofoil pressure distributions and drag for attached flows but, where flow separation is approached, the method is less reliable. The inadequacy of the method for flows of this type stems in part from the use of the concepts of first-order boundary-layer theory.

More recent developments have included methods for solving the Euler equations[3,4] in the inviscid part of the flow and others yielding solutions of the Reynolds-averaged Navier-Stokes equations[5,6]. The former class of methods retains the viscous-inviscid interaction procedure and thus needs allowance for effects which become important in regions approaching separation; the latter class is less restricted in this sense but currently relies on primitive turbulence models[7]. Thus methods of this type are not, at present, suitable for routine application.

In order to remedy the defects in VGK mentioned above, improvements have been made to the method to allow for 'higher-order' effects and other influences which become important in separated-flow regions. A first attempt to include these effects (to give a code known as AVGK) was not entirely successful because of the slowness of the numerical convergence of the 'direct' method (used to couple the inviscid and viscous flow solutions) as separation is approached. East *et al*[8] showed that, in such circumstances, an 'inverse' scheme for calculating the shear layers is preferable. In this scheme, boundary-layer displacement thickness (or 'wall' transpiration velocity) is assumed known and the wall streamwise-velocity distribution of the inviscid flow is calculated; this distribution is then used in the inviscid flow either directly as the wall boundary-condition or indirectly via an intermediate expression to define the wall transpiration velocity. The latter 'semi-inverse' procedure is employed in an improved version of AVGK known as BVGK[9]; thus AVGK is superseded by BVGK and so no further mention is made of AVGK in this paper.

The remainder of this paper starts with a description in section 2 of the aerofoils studied, follows this with a discussion of the experiment, including

the test techniques, in section 3, and continues by describing the main features of BVGK in section 4. Finally, predictions by VGK and BVGK of aerofoil pressure distributions and drag are compared with those of measurement in section 5.

2 Aerofoil Design

As noted in the Introduction, three families of aerofoils have been tested, and in this section characteristics of each family are briefly summarised. Each family is distinguished by the pressure distribution or shape of the rear half of the upper surface. In other respects the aerofoils, which have a common section ahead of 65% chord, are similar. Details of section shape and rear pressure distribution calculated by BVGK for selected aerofoils are given in Fig 1.

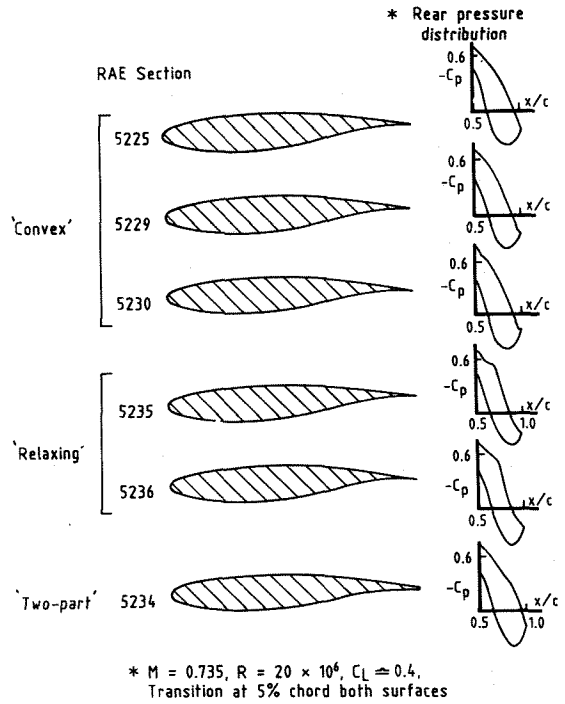

Fig.1 Families of aerofoils studied

2.1 Convex

The convex family of sections is so named because the pressure gradient on the upper surface increases monotonically with streamwise distance between about 60% and 80% chord. Six sections have been investigated in this family, three with sharp trailing edges, RAE 5225, RAE 5229 and RAE 5230, and the remainder with blunt bases. However, only those sections with sharp trailing edges are considered in this paper.

Of the three sharp trailing-edge aerofoils, RAE 5225 has the least tendency towards separation on the upper surface; this section is designed so that, at a lift coefficient $C_L = 0.6$, a free-stream Mach number $M_\infty = 0.735$, a chord Reynolds number $R = 20 \times 10^6$ and with transition at 5% chord on both surfaces, separation is just avoided near the trailing edge on the upper surface. RAE 5230 is the most extreme of the three, having been designed to have boundary-layer characteristics near the trailing edge on the upper surface at $R = 20 \times 10^6$ similar to those of RAE 5225 at $R = 6 \times 10^6$.

2.2 Relaxing

The name relaxing is used for these sections because the pressure gradient on the upper surface decreases or 'relaxes' with streamwise distance between 75% and 90% chord. This type of section has a possible advantage over more conventional sections for wings designed for high-speed cruise, since the upper-surface shape between 55% and 75% chord is such that shocks forming in this region are relatively weak at a given angle of incidence. Of the two relaxing sections, RAE 5236 is the more severe in terms of proximity to separation but is less prone to separation than all the convex sections. Despite this, RAE 5236 has a higher drag at a given lift at $M_\infty = 0.735$ than does the least extreme convex section RAE 5225, as is shown later.

2.3 Two Part

The pressure distribution on the upper surface of the solitary two-part section, RAE 5234, is characterised by a region of modest, adverse pressure-gradient between 60% and 90% chord followed downstream by a pronounced increase in pressure gradient. A novel feature of this section, which has a ½% thick base, is that it has a relatively large cross-sectional area aft of 55% chord, offering possible structural advantages and some freedom to design a flap with a generous nose radius.

3 Wind Tunnel Tests

3.1 Model and Measurement Techniques

The model was of 0.635 m chord for all aerofoil sections and spanned the tunnel working section, giving an aspect ratio of 3.84 and a chord to height ratio of 0.26. Special efforts were made to seal the two spanwise extremities.

Boundary-layer transition was fixed by means of the air-injection technique in which air is bled into the boundary layer through a row of small holes, drilled normal to the surface, at a rate just sufficient to fix transition. Details of the system are given in Fig 2 which also shows the construction of the model; further information is provided in Ref 10 where it is shown that, above a critical mass flow, transition is effectively fixed at the row of air holes at 5% chord on both surfaces,

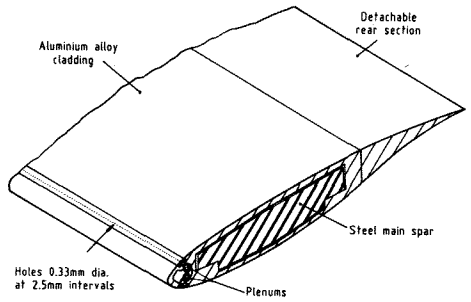

Fig. 2 Isometric view of model showing air-injection system

and evidence is presented suggesting that the spurious drag associated with air injection is negligible.

Surface static pressures were measured at orifices of 0.5 mm diameter and drilled normal to the surface both on the model centre line and at a limited number of positions on lines about one chord either side of the centre line. The off-centre holes were provided as a check on the spanwise uniformity of the flow but in this paper only pressures measured at the centre-line are considered.

Section lift and pitching moment were determined by appropriate integrations of the static pressures around the section contour. Section drag was determined from the momentum deficit in the wake far downstream; this deficit was inferred from measurements of total and static pressures made with a rake of pitot and static tubes located at the vertical plane of symmetry about two chords downstream of the trailing edge.

Details of the corrections applied to the data for static-hole error, tunnel-wall constraint and model static aeroelastic distortion are given in Ref 11. All the data presented in this paper are corrected for these effects. In particular, a simple correction for blockage is applied to free-stream Mach number and static pressure on the basis that the blockage increment in Mach number varies slowly along the aerofoil chord. On the other hand, a wall constraint correction to model incidence alone is not justified because of significant variations in wall-induced upwash in the region of the model. Therefore, in the comparisons between calculation and measurement to be discussed in section 5, an allowance is made for this variation by a correction to the aerofoil camber in the calculation, using the analogy between flow curvature and aerofoil camber suggested by linearised aerofoil theory[12].

The correction for model aeroelastic distortion arises because the model was free to rotate in a bearing at one spanwise extremity while being constrained at the other end by the incidence adjustment device. This arrangement avoided the complication of a following mechanism but meant that the model twisted under aerodynamic load. The correction to centre-line incidence was deduced from a prior static-calibration and from values of aerodynamic pitching-moment inferred from the static-pressure measurements. The same calibration indicated that the twist over the central 50% span was about half the change in centre-line incidence.

Limited checks were made of the spanwise variation of section drag coefficient by rotating the wake rake about its axis through the wake for a number of shock-free flows. Differences between the centre-line value and values at between 0.3 and 0.5 chords either side of the centre-line were found to be small, typically from 0.0001 to 0.0002.

An assessment of the effect of various sources of error suggests that static pressure and drag coefficients are accurate to within ±0.002 and ±0.0001, respectively. A high standard of repeatability was achieved in the measurement of pressure both between and within test series, static pressure and drag coefficients being repeatable to within ±0.001 and ±0.0001.

3.2 Test Conditions

The measurements were made for free-stream Mach numbers within the range 0.5 to 0.75 and for chord Reynolds numbers from 6×10^6 to 20×10^6 for all sections except RAE 5230 for which the maximum Reynolds number was 17.7×10^6. All the tests described here were made with transition fixed, established by varying air-injection mass flow until there was no further change in drag with mass flow.

4 Calculation Method

BVGK contains the same basic procedures as VGK, including the lag-entrainment method[13] for calculating the turbulent shear-layers, but embodies changes to the modelling of the shear layers which become increasingly important as separation is approached and uses a revised method to couple the viscous and inviscid flow solutions.

4.1 Improvements to the Modelling of Viscous Effects

The changes to the modelling of the shear layers in BVGK are:

(a) Allowance for 'higher-order' effects in the equations for integrated shear layer mass and momentum deficit due to flow curvature and, where appropriate, second-order Reynolds stresses.

(b) A revised shape-parameter relationship which is more suitable for flows with separation.

(c) Modifications to improve the accuracy of the skin friction and the shape parameter of the velocity profile at low local Reynolds number.

(d) Allowance for the effect on turbulence structure of flow curvature (a correction which is available in the lag-entrainment method but not implemented in VGK).

4.1.1 Higher-order effects

By differencing the respective equations of continuity and Reynolds-averaged, Navier-Stokes equations for two flows - the Equivalent Inviscid Flow (EIF) and the Real Viscous Flow (RVF) - East[14] was able to adapt the equations for integrated mass and momentum deficit in the shear layers to include higher-order effects. The former flow coincides with the latter where the flow is inviscid and is the smooth continuation of the inviscid flow within the shear layers. He obtained for the wall transpiration velocity in EIF

$$W_{iw} = \frac{1}{\rho_{iw}} \frac{d}{ds} (\rho_{iw} U_{iw} \delta^*) \quad , \qquad (1)$$

where suffixes i and w refer to EIF and to wall (aerofoil contour or rear dividing streamline) conditions, U is velocity in the streamwise direction s and

$$\delta^* = \frac{1}{\rho_{iw} U_{iw}} \int_0^{\delta} (\rho_i U_i - \rho U) dz \qquad (2)$$

is generalised displacement thickness. The integration indicated in equation (2) is performed from the wall ($z = 0$) to the outer edge of the shear layer ($z = \delta$) along a normal to the wall.

Defining a generalised momentum thickness

$$\theta = \frac{1}{\rho_{iw} U_{iw}^2} \int_0^{\delta} [\rho U (U_{iw} - U) + \rho_i U_i (U_i - U_{iw})] dz$$

and ignoring terms which are significant only when surface curvature is large and the boundary layer grows rapidly, East showed that the streamwise momentum integral equation may be expressed as

$$\frac{d\theta}{ds} + (H + 2 - M_{iw}^2) \frac{\theta}{U_{iw}} \frac{dU_{iw}}{ds} - \frac{C_f}{2} = - \frac{1}{\rho_{iw} U_{iw}^2} \frac{d(\rho_{iw} U_{iw}^2 f\theta)}{ds} + \frac{M_{iw}^2}{U_{iw}^2} \theta W_{iw} \frac{dW_{iw}}{ds} \quad . \qquad (3)$$

Here C_f is an equivalent skin friction coefficient, M is Mach number and $H = \delta^*/\theta$. The term f may be expressed as the sum of two terms due respectively to flow curvature and to Reynolds normal stresses.

Equations (1) and (3) differ from the standard first-order expressions in VGK in that the inviscid-flow quantities are defined by wall conditions in EIF rather than by those at the outer edge of the shear layer (which in VGK are inferred from the wall static pressure of RVF using the boundary-layer approximation $\partial p/\partial z = 0$, where p is static pressure). Lock and Firmin[15] argued that this change is equivalent to an increase in adverse pressure-gradient in regions of rapid boundary-layer growth such as near the trailing edge. An additional difference is that the right-hand side of equation (3) is non-zero, in general, whereas it is zero in the first-order equation.

The second term on the right-hand side of equation (3) is generally less important than the first and is thus neglected. Consistent with this approximation, U_{iw} is assumed equal to the surface speed in EIF, $q_{iw} = \sqrt{U_{iw}^2 + W_{iw}^2}$. A study of the errors in boundary-layer thicknesses involved in using q_{iw} instead of U_{iw} suggests that they may be ignored for the flows considered in this paper.

In a similar way, East derived the normal momentum-integral equation and from it showed that wall static pressures in the two flows are related by the expression

$$p_{iw} - p_w = \kappa^* \rho_{iw} U_{iw}^2 (\theta + \delta^*) \quad ,$$

where κ^* is the displacement-surface curvature. For convenience, this equation is not used directly in BVGK but is combined with the usual linearising assumptions to derive a flow speed corresponding to p_w

$$q_w = U_{iw} [1 + \kappa^* (\theta + \delta^*)] \quad . \qquad (4)$$

In principle, equation (4) allows a solution to be obtained for the inviscid flow which is compatible with the Kutta condition of smooth flow at the trailing edge expressed as

$$(q_w)_u = (q_w)_l \quad ,$$

suffixes u and l referring to the upper and lower surfaces approaching the trailing edge. However, the conformal transformation used in the calculation of the inviscid flow is such that the solution for the flow is not defined at the trailing edge. The method used to solve

this problem within the framework of the revised treatment of the shear layers is described later.

Modifications to the entrainment and lag equations in the lag-entrainment method consequent on the use of EIF wall quantities in the definition of the integral thicknesses are described in Ref 9.

4.1.2 Shape Parameter Relationship

In the lag entrainment method, the mass-flow shape parameter

$$H_1 = \int_0^{\delta} \rho U dz / \rho_{iw} U_{iw} \theta$$

and the transformed shape parameter

$$\overline{H} = \int_0^{\delta} \rho (U_{iw} - U) dz / \rho_{iw} U_{iw} \theta$$

are related by the expression

$$H_1 = 3.15 + 1.72/(\overline{H} - 1) - 0.01(\overline{H} - 1)^2 \quad .$$

This formula is intended to represent a wide range of aerofoil flows but is biased towards those with severe, adverse pressure gradients. The last term on the right-hand side is intended to ensure that $dH_1/d\overline{H}$ is finite for all positive $\overline{H}$, thus avoiding singular behaviour in the integration of the shear-layer equations by the direct method.

In BVGK an alternative relationship is used

$$H_1 = 2 + 1.5/(\overline{H} - 1) + 0.5(\overline{H} - 1), \quad 1.3 < \overline{H} < 4 ;$$

$$H_1 = 4 + \tfrac{1}{3}(\overline{H} - 4), \quad 4 < \overline{H} < 12 \quad . \quad (5)$$

Equation (5) displays a minimum in H_1 at a value of $\overline{H}$ (= 2.7) close to that for incipient separation. As implied above, relationships of this type cannot be used for the calculation of separated flows by the direct method normally associated with the lag-entrainment method but pose no problem when the inverse method is used. Lock[16] showed that an expression similar to equation (5) is suitable for low-speed flows, and it would appear that the same is true of flows at high subsonic speed except in regions of sudden and severe pressure gradient[17] (eg strong shock waves).

4.1.3 Skin-Friction Relationship

The skin-friction coefficient C_f is assumed to be equivalent to the standard definition but the formula used differs from that of the lag-entrainment method in two respects:

(a) Allowance is made for the effects of low Reynolds number on the velocity profile of the turbulent shear layer.

(b) A lower limit of -0.0002 is imposed on the skin friction coefficient.

The first modification, which is described in detail in Ref 9, is made to allow for changes in the character of turbulent boundary-layers at low Reynolds number (ie at a momentum-thickness Reynolds number R_θ below about 5000), relative to that at higher Reynolds number, originally observed by Coles[10].

According to Preston[19], a flat-plate boundary layer with fully-developed turbulence is not possible for values of R_θ less than 320 in low speed flows. In view of this, and in the absence of evidence on the effects of pressure gradient and compressibility, this value has been taken to be the lower limit of R_θ just downstream of transition, the momentum thickness there being adjusted accordingly when necessary.

4.1.4 Curvature Effects on Turbulence Structure

A method allowing for the influence on turbulence structure of streamwise flow curvature is described by Green et al[13]. This correction with a modification proposed by Bradshaw[20] to allow for a lag of 10δ can be included in BVGK. The mean value of flow curvature across the shear layer used in this correction is taken to be that of the displacement surface. It is doubtful if this approximation is valid for separated flows where the variation of flow curvature across the layer is likely to be large. This aspect of the method is considered again in section 5 where calculation and measurement are compared.

4.2 Viscous-Inviscid Interaction Procedure

BVGK is semi-inverse in character since it uses an inverse method to calculate the turbulent shear layers but applies the wall transpiration condition in the calculation of EIF as in the conventional direct scheme. In both VGK and BVGK the method of Garabedian and Korn is used to calculate the inviscid flow with a modification to the numerical difference scheme by Lock[2] to improve the representation of shocks. However, in BVGK a different method is used to satisfy the Kutta condition and this is described later.

4.2.1 Calculation of Shear Layers and Viscous-Inviscid Matching

On each surface, the laminar boundary layer and the turbulent boundary layer to one grid point downstream of transition are calculated in the usual direct way. Further downstream, the inverse method is used whereby δ^* is specified and U_{iw} is determined along with other boundary-layer parameters, the iteration process being started with an assumed distribution of displacement thickness.

Matching between the inverse part of the solution and EIF is accomplished with an expression due to Carter[21]

$$\delta^*(n+1) = \delta^*(n)\left(1 + \Omega\left(\frac{U^V_{iw}}{U^I_{iw}} - 1\right)\right),$$

where superscripts I and V refer to the previous inviscid solution and to the solution of the shear layers, n is the number of viscous iterations and Ω is a relaxation factor. Wall transpiration velocity is then obtained from equation (1) with ρ_{iw} and U_{iw} being derived from the inverse solution of the shear layers.

4.2.2 Treatment of Trailing Edge and Wake

The conformal mapping used in the calculation of EIF is singular at the trailing edge, and thus the solution of EIF is not defined at this point. Hence, without further consideration, it is not possible either to match the two flow solutions there using Carter's formula or to satisfy the Kutta condition directly. The method used to solve this problem is as follows. First, a further approximation to δ^* at the trailing edge is found by a smooth interpolation of the displacement surface (Fig 3). For this purpose, the wake centre line near the trailing edge is taken to be a straight line, initially assumed to be parallel to the reference streamwise axis of the aerofoil. Second, having determined displacement-surface curvature at the trailing edge on each surface by interpolation, flow speeds corresponding to RVF pressures at the trailing edge are found using equation (4). At this stage, the Kutta condition is not necessarily satisfied; therefore the angle of the wake centre-line relative to the reference axis, ψ, is adjusted after each shear-layer calculation until values of δ^* at the trailing edge are obtained which are consistent both with the Kutta condition and the requirement of a smooth displacement surface.

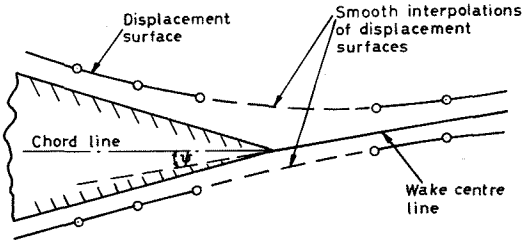

- Smooth displacement surface
- Kutta condition

Fig.3 Flow conditions to be satisfied at trailing edge

The condition of zero pressure difference across the wake centre-line is also imposed further downstream. As shown by Lock[16], this condition defines the jump in velocity across the wake in EIF.

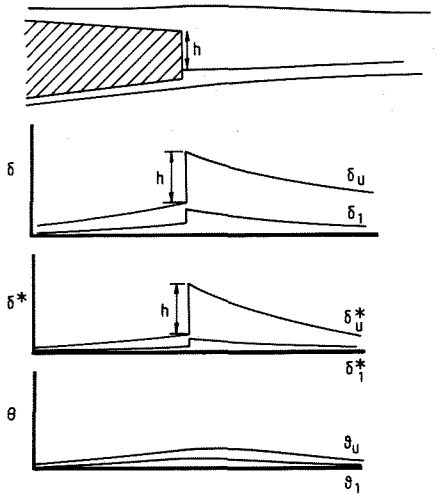

Fig.4 Streamwise variation of shear - layer thickness near trailing edge of blunt-base aerofoil

The effect of a blunt base is incorporated in a simple way as follows. As before, the displacement surface is taken to be continuous at the trailing edge, and the unique shape-parameter relationship, equation (5), is retained. Fig 4 illustrates the streamwise distributions of the shear-layer parameters upstream and downstream of the trailing edge. Both the thickness δ_u and displacement thickness δ_u^* of the shear layer above the rear dividing streamline increase discontinuously at the trailing edge by the amount h, the height of the trailing edge of the upper surface above the intersection of the dividing streamline with the base. This implies that $H_u = \delta_u^*/\theta_u$ jumps at the trailing edge by the amount h/θ_u, while $(H_1)_u = (\delta_u - \delta_u^*)/\theta_u$ is continuous there. A similar argument applies to the shear layer below the dividing streamline (Fig 4). Since the value of H_1 of

either shear layer just downstream of the trailing edge is not necessarily consistent with that implied by the shape-parameter relationship, an adjustment is made to H_1 where necessary as illustrated in Fig 5. The position of the dividing streamline on the base, which determines the values of the boundary-layer thicknesses either side of the wake, is unknown; however, overall forces are found to be insensitive to changes in this position. Therefore in the calculations on the blunt-base aerofoil RAE 5234 the height h is taken to be 90% of base thickness.

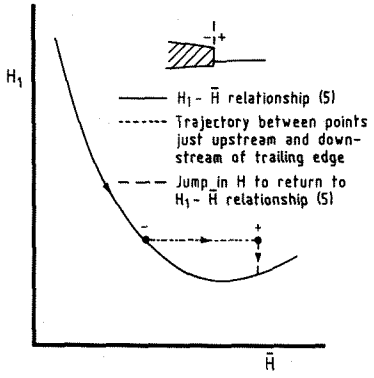

Fig.5 Adjustment to mass - flow shape parameter just downstream of trailing edge

The wake boundary conditions in EIF are applied on the chordwise extensions of the edges of the base in the way described by Lock and Williams[22].

5 Comparison Between Calculation and Experiment

Full details of the calculation procedure are given in Ref 9. Nominal (design) ordinates were used in the calculations; the errors in the ordinates are small with a magnitude of less than 0.0002c, where c is aerofoil chord. The associated errors in surface pressure are calculated to be negligible except close to sonic conditions.

Drag is calculated using the expression

$$C_D = C_{D_V} + C_{D_W} ,$$

where

$$C_{D_V} = 2\theta_f/c$$

is the viscous drag coefficient, suffix f referring to conditions far downstream. The wave-drag coefficient C_{D_W} is calculated by a procedure[23] which identifies conditions just upstream of the shock in the flowfield and infers a shock total-pressure loss from that of a Rankine-Hugoniot shock of the same Mach number normal to and just upstream of the shock. Wave drag then follows from application of the momentum theorem to stream-tubes downstream of the shock on the assumption of adiabatic, isentropic flow.

5.1 Convex Sections

Calculated and measured pressure distributions are shown in Figs 6 and 7 for $M_\infty = 0.735$, $C_L = 0.6$ and for two Reynolds numbers $R = 20 \times 10^6$ (or 17.7×10^6 for RAE 5230) and 6×10^6. These flows have a supercritical region above the upper surface commencing close to the leading edge and terminating in a weak shock at about 50% chord. In some cases, re-expansion of the flow is evident upstream of the shock. All the flows are sensitive to errors in

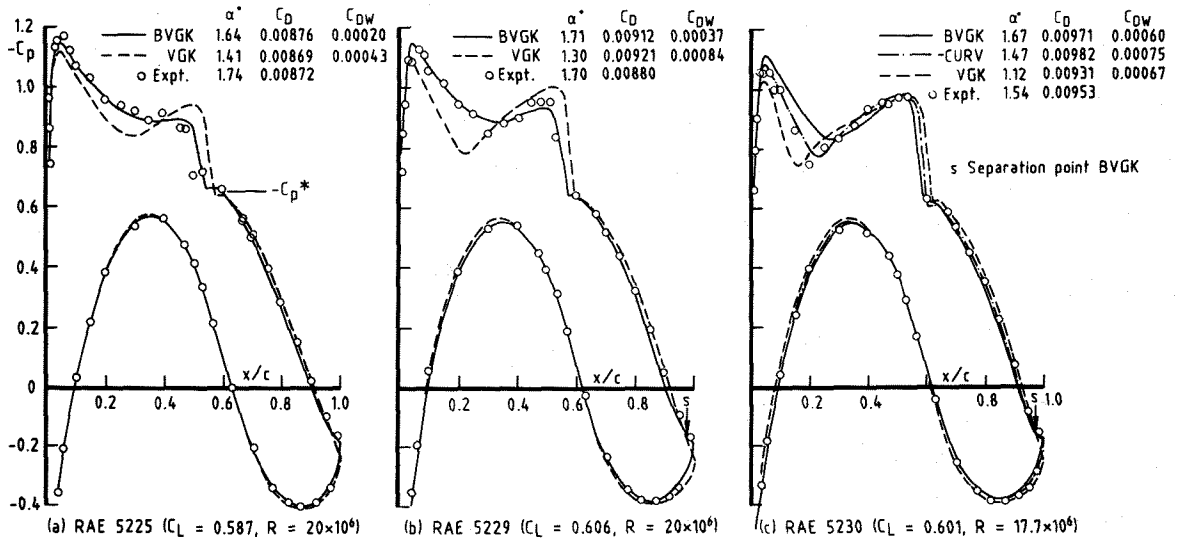

(a) RAE 5225 (C_L = 0.587, R = 20×10⁶) (b) RAE 5229 (C_L = 0.606, R = 20×10⁶) (c) RAE 5230 (C_L = 0.601, R = 17.7×10⁶)

Fig.6 Calculated and measured pressure distributions for 'Convex' sections, M_∞=0.735

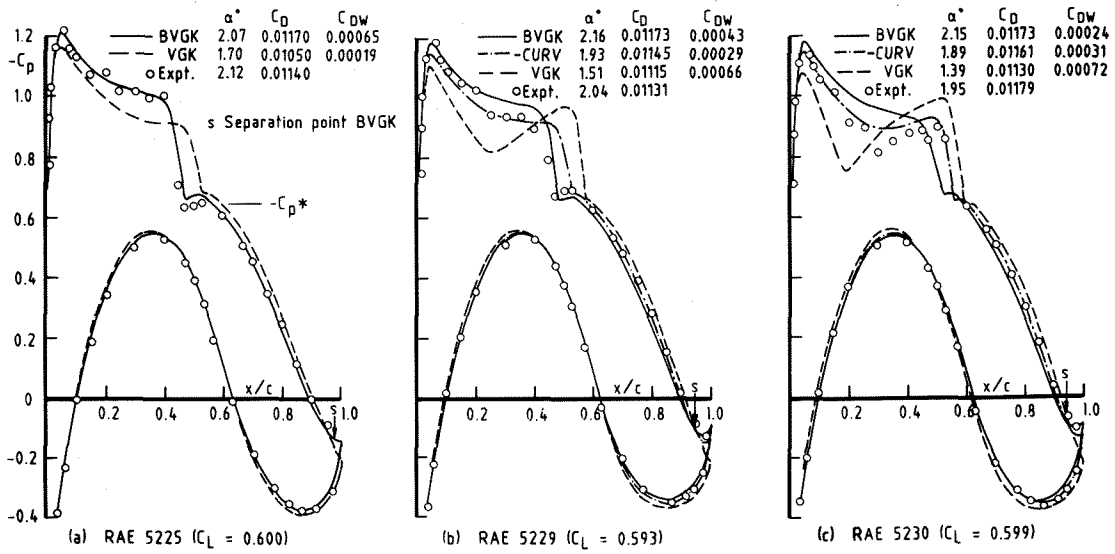

Fig.7 Calculated and measured pressure distributions for 'Convex' sections, M_∞=0.736, R=6×10⁶

EIF boundary conditions and are thus good tests of the accuracy of the modelling of the shear-layer displacement effect. The calculations are made at the measured lift but the calculated incidence and drag are compared with the experimental values in the figures.

BVGK gives excellent predictions of pressure distributions and angle of incidence for RAE 5225 at both Reynolds numbers and for RAE 5229 at R = 20 × 10^6. The improvement in agreement with experiment compared with VGK is especially evident for the two cases with separation calculated by BVGK to occur at about 2% chord upstream of the trailing edge on the upper surface (Figs 6b and 7a). In these cases, VGK overestimates the rear loading with a consequent effect on the prediction of both the pressures in the supercritical flow region and angle of incidence. For the flows with separation calculated to occur at between 95% and 97% chord on the upper surface (Figs 6c, 7b and 7c), BVGK underestimates the rear loading and hence does not provide as close a prediction of the supercritical pressures as in the other flows. This discrepancy is believed to arise from the inadequacy of the correction for the effect on turbulence structure of the flow curvature in flows with significant regions of separation (ie of chordwise extent greater than about 2% chord), as foreshadowed in section 4.1.4. In such cases, a marked improvement in agreement with measurement is obtained in respect of the suction levels upstream of the shock if this correction is ignored (-CURV).

Further validations of pressure distributions calculated by BVGK for sections RAE 5225 and 5230 are presented in Ref 9.

Comparisons between calculated and measured overall forces and pitching moment for the same Mach number* and Reynolds number of Figs 6 and 7 are shown in Fig 8. BVGK is seen to give much improved estimates of overall forces compared with those of VGK, particularly at the lower Reynolds number. The improvement in agreement in the predictions of

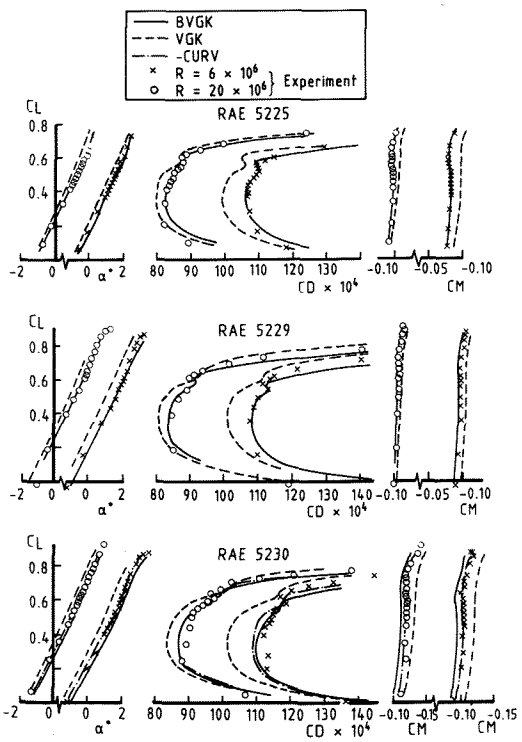

Fig.8 Lift, drag and pitching moment, 'Convex' sections, M_∞ ≙ 0.735, R = 6 × 10^6 & 20 × 10^6 (17.7 × 10^6 for RAE 5230)

* In the tests, Mach number was allowed to change slightly during incidence traverses but all the calculations have been made at the appropriate Mach number.

drag by BVGK over those of VGK is especially noteworthy. For flows without shock waves, the predictions of drag coefficient by BVGK are generally within about 0.0001 of the measured value. On the other hand, at higher or lower incidences than those for shock-free flow, the estimates of drag by BVGK are not as good. The discrepancies at higher incidences ($C_L > 0.6$) are especially evident for the flow with the largest region of separation (RAE 5230, $R = 6 \times 10^6$). As noted before, BVGK underestimates the rear loading for such flows, and hence predicts higher suctions than those of measurement upstream of the shock at a given lift with the consequence that the method overestimates wave drag. Some improvement in agreement between calculation and measurement is obtained for lift coefficients greater than about 0.6 for RAE 5230 at $R = 6 \times 10^6$ if the curvature correction to turbulence is neglected as shown in Fig 8.

Another possible source of error arises from the assumption of the wave-drag procedure that the local flow is normal to the shock. This assumption is likely to result in an overestimate of wave drag in real flows where the shock is oblique close to the aerofoil surface.

5.2 Relaxing Sections

Pressure distributions at corresponding conditions to those of Figs 6 and 7 are shown in Figs 9 and 10 for the 'relaxing sections, the flows over which are all predicted by BVGK to be attached on both surfaces. BVGK is seen to give accurate estimates of the pressure distributions aft about 60% chord but discrepancies between predictions by BVGK and measurement are apparent in and just downstream of the supercritical-flow region on the upper surface. However, BVGK gives improved estimates of pressure distributions compared with those of VGK, particularly at the lower of the two Reynolds numbers (Fig 10). Figs 9 and 10 show that BVGK estimates of drag are also significantly closer to the measured values than those of VGK. Further, more detailed, comparisons of overall forces are shown in Fig 11 for the nominal Mach number and Reynolds number of Figs 9 and 10. Fig 11 confirms the improved accuracy of the predictions of drag by BVGK compared with those of VGK. For both sections, BVGK predictions of drag coefficient are within about 0.0001 of the measured values over the range $0.2 \leq C_L \leq 0.6$. BVGK is also seen to give

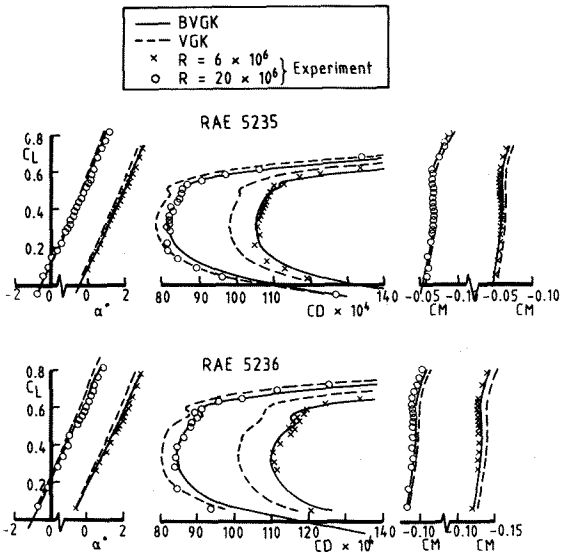

Fig.11 Lift, drag and pitching moment, 'Relaxing' sections, $M_\infty \simeq 0.735$, $R = 6 \times 10^6$ and 20×10^6

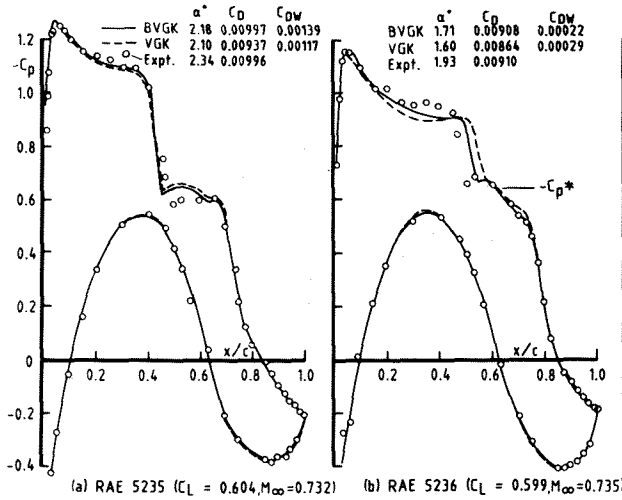

(a) RAE 5235 ($C_L = 0.604, M_\infty = 0.732$) (b) RAE 5236 ($C_L = 0.599, M_\infty = 0.735$)

Fig.9 'Relaxing' sections, calculated and measured pressure distributions, $R = 20 \times 10^6$

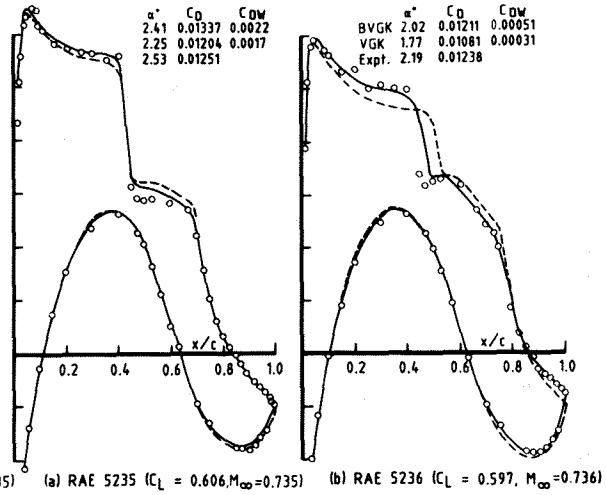

(a) RAE 5235 ($C_L = 0.606, M_\infty = 0.735$) (b) RAE 5236 ($C_L = 0.597, M_\infty = 0.736$)

Fig.10 'Relaxing' sections calculated and measured pressure distributions, $R = 6 \times 10^6$

the more accurate estimates of lift at a given angle of incidence and pitching-moment at a given lift.

Comparison between Figs 8 and 11 shows that RAE 5236 has larger drag at a given lift than that of the convex section RAE 5225. This occurs in spite of the flow being calculated to be attached on the former section and separated at 98% chord on the upper surface of the latter.

5.3 Two-Part Section

Pressure distributions (for $M_\infty \approx 0.73$, $C_L = 0.6$) and overall forces and pitching moment for the two-part section RAE 5234 are shown in Figs 12 and 13. As with the other sections, BVGK is seen to give accurate estimates of drag over a range of lift coefficients which is useful for design purposes and to provide significantly improved predictions of pressure distributions, lift, drag and pitching moment compared with those of VGK.

Overall, the agreement between BVGK predictions and measurement is good for all sections, except at high and low lift when strong shocks appear. Attention is drawn, in particular, to the accuracy of the estimates of differences in 'subcritical' drag between the sections of all three families and between Reynolds numbers for a given section. This illustrates the possible use of the method as a design tool and also for 'extrapolating' wind-tunnel data for wing sections to 'full scale'.

6 Conclusions

A combined theoretical and experimental investigation of transonic flows over three families of advanced aerofoils with various rear-pressure distributions has been described. In the experiment, special care was taken to ensure that the data were of sufficient quality to allow rigorous validation of CFD methods. A large number of different flows were studied, ranging from those that were completely attached to those with regions of separation.

The data have been used to validate CFD methods developed at RAE including a viscous-inviscid interaction method known as BVGK. This method has been shown to predict accurately pressure distributions and section drag for a wide range of flows including those with rear separation, suggesting the use of the method as a tool for designing sections and extrapolating wind-tunnel data to 'full scale'.

Following extensive validation, BVGK is currently in use in UK aerospace industry. Eventually, the method will be replaced by more sophisticated methods but before they are accepted as design tools they will have to demonstrate an accuracy at least equal to that shown by BVGK.

References

1 P.R. Garabedian, D.G. Korn. "Analysis of transonic airfoils." Comm. Pure App Math, XXIV, pp 841-851, (1971).

2 M.R. Collyer, R.C. Lock. "Prediction of viscous effects in steady transonic flow past an aerofoil." Aero Qu, 30 485, (1979).

3 R.H. Doe, A. Pagano, T.W. Brown. "The development of practical Euler methods for aerodynamic design." ICAS 86 5.5, (1986).

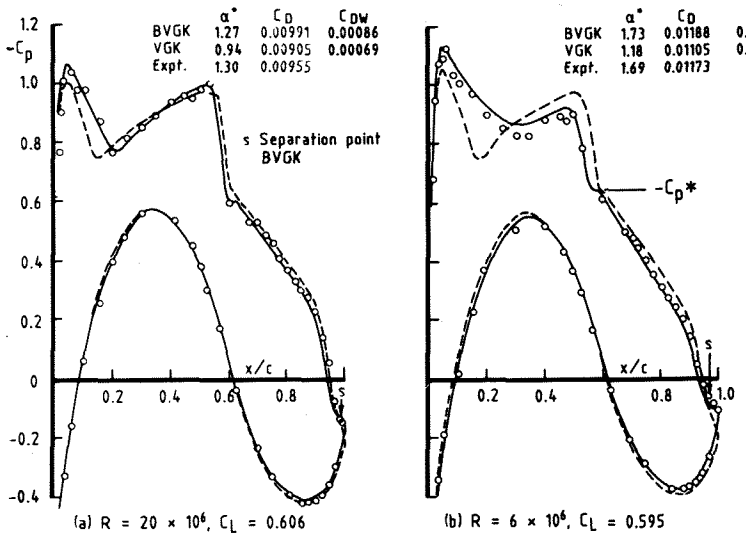

(a) $R = 20 \times 10^6$, $C_L = 0.606$ (b) $R = 6 \times 10^6$, $C_L = 0.595$

Fig.12 'Two-part' section RAE 5234, calculated and measured pressure distributions, $M_\infty = 0.736$

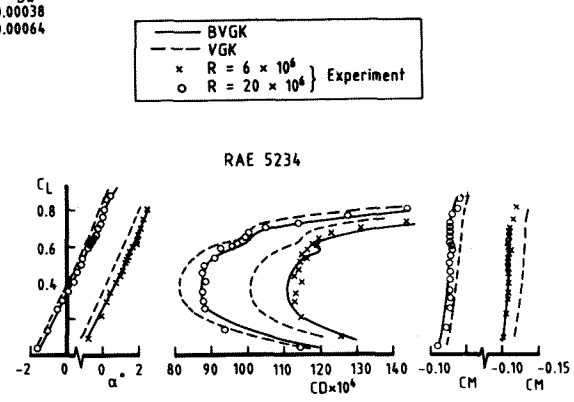

Fig.13 Lift, drag and pitching moment, 'two-part' section, $M_\infty \simeq 0.735$, $R = 6 \times 10^6$ and 20×10^6

4 L.T. Chen, S. Li, H. Chen. "Calculation of transonic airfoil flows by interaction of Euler and boundary-layer equations." AIAA Paper No 87-0521, (1987).

5 L.S. King. "A comparison of turbulence closure models for transonic flows about airfoils." AIAA Paper No 87-0418, (1987).

6 L.J. Johnston. "Some preliminary results from a prediction method for the viscous flow around aerofoil sections." ARA Memorandum 281, (1987).

7 T.L. Holst. "Viscous transonic airfoil workshop compendium of results." AIAA Paper No 87-1460, (1987).

8 L.F. East, P.D. Smith, P.J. Merryman. "Prediction of the development of separated turbulent boundary layers by the lag-entrainment method." RAE Technical Report 77046, (1977).

9 P.R. Ashill, R.F. Wood, D.J. Weeks. "An improved, semi-inverse version of the viscous, Garabedian and Korn method." RAE Technical Report 87002, (1987).

10 P.R. Ashill, J.L. Fulker, D.J. Weeks. "The air-injection method of fixing boundary-layer transition and investigating scale effects." The Aeronautical Journal 91, pp 214-224, (1987).

11 P.R. Ashill, D.J. Weeks, J.L. Fulker. "Wind tunnel experiments on aerofoil models for the assessment of computational flow method." AGARD-CPP-437, (1988).

12 P.R. Ashill, D.J. Weeks. "A method for determining wall-interference corrections in solid wall tunnels from measurements of static pressure at the wall." AGARD-CP-335 Paper 1, (1982).

13 J.E. Green, D.J. Weeks, J.W.F. Brooman. "Prediction of turbulent boundary layers and wakes in compressible flow by a lag entrainment method." ARC R&M 3791, (1973).

14 L.F. East. "A representation of second-order boundary layer effects in the momentum integral equation and in viscous-inviscid interactions." RAE Technical Report 81002, (1981).

15 R.C. Lock, M.C.P. Firmin. "Surveys of techniques for estimating viscous effects in external aerodynamics." In "Numerical methods in aeronautical fluid dynamics" (ed P.L. Roe), Academic Press, (1982).

16 R.C. lock. "Prediction of the drag of wings at subsonic speeds by viscous/inviscid interaction techniques." AGARD-R-723 "Aircraft drag prediction and reduction", (1985).

17 D.J. Weeks. RAE unpublished work.

18 D.E. Coles. "The turbulent boundary layer in a compressible fluid." USAF Project Rand Report R-403-PR, (1962).

19 J.H. Preston. "Minimum Reynolds number for a turbulent boundary layer and the selection of a transition device." Journal of Fluid Mechanics 3, Pt IV, pp 373-384, (1957).

20 P. Bradshaw. "Effects of streamline curvature on turbulent flow." AGARD AG 169, (1973).

21 J.E. Carter. "A new boundary layer inviscid iteration technique for separated flow." AIAA Paper 79-1450, (1979).

22 R.C. Lock, B.R. Williams. "Viscous-inviscid interactions in external aerodynamics." Prog Aerospace Sci Vol 24, pp 51-171, (1987).

23 C.M. Billing, A.J. Bocci. "The MACHCONT method for calculating the wave drag of a 2D aerofoil." ARA Memorandum 272, (1986).

Acknowledgment

The efforts of Mrs N. Rycroft and Mr G.L. Riddle in preparing the diagrams and Miss C.J. Betts in assisting with the calculations are gratefully acknowledged.